COMMUNICATION

Facile preparation of sulphur-doped graphene quantum dots for ultra-high performance ultraviolet photodetectors

Received 00th January 20xx,
Accepted 00th January 20xx

DOI: 10.1039/x0xx00000x
www.rsc.org/

Shuxiong Gao, [a] Libin Tang, *[b] Jinzhong Xiang, *[a] Rongbin Ji, *[b] Sin Ki Lai, [c] Shouzhang Yuan[b] and Shu Ping Lau [c]

Sulphur-doped graphene quantum dots (S-GQDs) were prepared in this work by a novel and facile method using the co-combustion (T-X-J method) of a liquid mixture of paraffin oil and carbon disulphide (CS_2). Ultra-high performance (*R*: 307 AW^{-1}; *D:1.5x10^{14} Jones) ultraviolet photodetectors based on S-GQDs were fabricated under ambient condition, shedding light on fabricating graphene based high-performance optoelectronic devices.**

Graphene quantum dots (GQDs), which are composed of only earth-abundant elements yet exhibit efficient photoluminescence, have attracted intense research attention in recent years due to its potential applications in optoelectronics and biomedicine. Numerous ways have been developed to synthesize GQDs, including nitric acid-assisted oxidation of graphene,[1] microwave-assisted hydrothermal method,[2] electrochemical etching of graphite.[3] Many of these synthetic methods require harsh chemical conditions, which are harmful to the environment; and/or rely on special equipment like electrical and microwave generators. Although semiconductor quantum dots (QDs), e.g. PbS QDs,[4,5] CdSe QDs,[6,7] have shown higher performance than GQDs for solution processable optoelectronic devices up to date, they contain toxic elements which impose critical concern on environmental pollution and human safety for large-scale production.

GQDs is a potential candidate as an environmental-friendly solution processable optoelectronic material as it does not contain harmful or scarce elements, while development of a green, low-cost synthetic method can make GQDs even more suitable for large-scale optoelectronic applications than semiconductor QDs. In this work, sulphur-doped GQDs were synthesized by an all-green process of the co-combustion of a liquid mixture of paraffin oil and carbon disulphide (CS_2), serving as the carbon and sulphur source in S-GQDs respectively, in a low-cost alcohol lamp. The synthesis process is schematically depicted in Fig. 1a. Furthermore, our group has recently reported that sulphur doping can effectively alter the electronic structure and optical absorption of GQDs.[8]

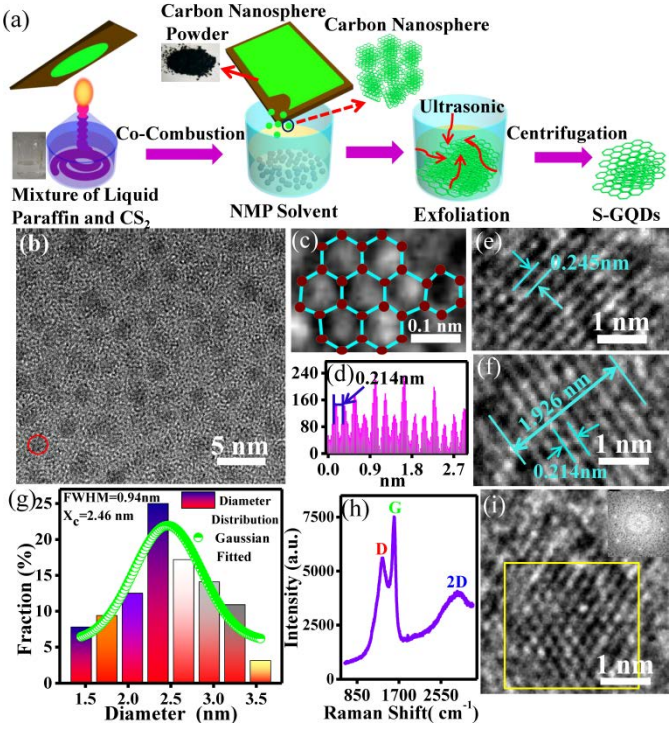

Fig. 1 (a) Schematic representation of the synthesis of S-GQDs. (b) TEM image of the as-prepared S-GQDs. (c) The HR-TEM image of the selected area (red circle), the hexagonal honeycomb structure was indicated. (d) The line-profile analysis of the S-GQD as shown in (f). (e) and (f) The HRTEM image of the S-GQDs with lattice fringe spacings of 0.245 nm and 0.214 nm. (g) The size distribution of the S-GQDs. (h) The Raman spectrum of the S-GQDs film on Si substrate. (i) An enlarged image showing the selected quantum dots in Figure 1b. Inset: the FFT pattern of the selected area (yellow box).

Un-doped GQDs has a large bandgap with absorption peak at deep ultraviolet (~280 nm).[9-11] Sulphur doping enhance the absorption of GQDs at the ultraviolet region and a set of high performance photodetectors operated at 365 nm have been successfully fabricated from the S-GQDs synthesized by this low-cost and all-green route.

[a] *School of Materials Science and Engineering, Yunnan University, Kunming 650091, People's Republic of China; E-mail: jzhxiang@ynu.edu.cn*
[b] *Kunming Institute of Physics, Kunming 650223, People's Republic of China; E-mail: scitang@163.com*
[c] *Department of Applied Physics, The Hong Kong Polytechnic University, Hung Hom Kowloon, Hong Kong*

Electronic Supplementary Information (ESI) available: The PL emission spectra of the S-GQDs aqueous solution in Fig. S1. Device performance of PVK-sole UV detector in Fig. S2. The Analysis of the optical properties of PVK in Figure S3, and comparison of the performances of UV photodetectors based on carbon nanomaterials in Table S1. See DOI: 10.1039/x0xx00000x

The S-GQDs were imaged under transmission electron microscope (TEM) as shown in Fig. 1b. The quantum dots are spherical in shape and distributed homogeneously without aggregation. The size distribution of the S-GQDs was analyzed in Fig. 1g, which follows a Gaussian distribution as indicated by the green fitting curve. The average diameter of the S-GQDs is 2.46nm with a FWHM of 0.94 nm. This shows that the S-GQDs have a narrow size distribution that confirms the homogeneity of the GQDs fabricated by this facile method. Fig. 1i shows the enlarged area from the red circle indicated in Fig. 1b, where for a region (yellow box), fast Fourier Transform (FFT) was performed as shown in the inset. It can be seen that the S-GQDs possess a hexagonal crystal structure anticipated from graphene.[12-14]The selected area in the yellow box is enlarged ten times and shown in Fig. 1c. The atoms are explicitly identified and marked out, which clearly demonstrated the hexagonal arrangement of atoms identical with graphene structure.[15] Fig. 1e and 1f show the typical high resolution TEM (HR-TEM) images from two randomly chosen S-GQDs. Lattice fringes which appear as bright dots can be clearly observed, indicating the good crystallinity of our S-GQDs. The lattice planes spacing of 0.245 nm and 0.214 nm represents the (100) and (110) planes of graphite respectively.[16,17] Fig. 1d shows the line profile of the lattice planes in Fig. 1f. It is verified that the separations among planes are of equal distances of 0.214 nm. The Raman spectrum of the S-GQDs is shown in Fig. 1h. Three prominent peaks including the D peak (1346 cm^{-1}),[18] G peak (1608 cm^{-1}) and 2D peak (2882 cm^{-1}) can be observed. In particular, the significant 2D peak represents the presence of relatively large domain of highly ordered sp^2 carbon in the S-GQDs and a low defect density in the S-GQDs.

Fig. 2a shows the scanning electron microscopy (SEM) image of the solid S-GQDs film, and the inset is the magnification from a selected area. It shows that the dense, thick film of S-GQDs comprised of spherical nanoparticle of size ~20 nm. A similar morphology of the film is further confirmed by atomic force microscope (AFM) in Fig. 2e. The elemental analysis in the S-GQDs was carried out using the energy dispersive spectroscopy (EDS) as shown in Fig. 2b. The S-peak indicates that presence of sulphur in S-GQDs. A small O-peak represents a low density of oxygen functional group in GQDs synthesized by this bottom-up method, which maybe relate to a lower number of oxy-groups in the carbon basal plane and lead to a long range sp^2 order as reflected by the prominent 2D peak in the Raman spectrum. The functional groups are investigated in the Fourier Transform Infrared (FTIR) spectrum in Fig. 2c. The peaks at 690 and 1173 cm^{-1} corresponds to the C-S and C=S bonds respectively,[8] which indicate the successful doping of sulphur into the GQDs through covalent bonding with carbon. Two other peaks at 1390 and 1630 cm^{-1} are attributed to the C-C and C=C bonds respectively.[19,20] The x-ray diffraction (XRD)

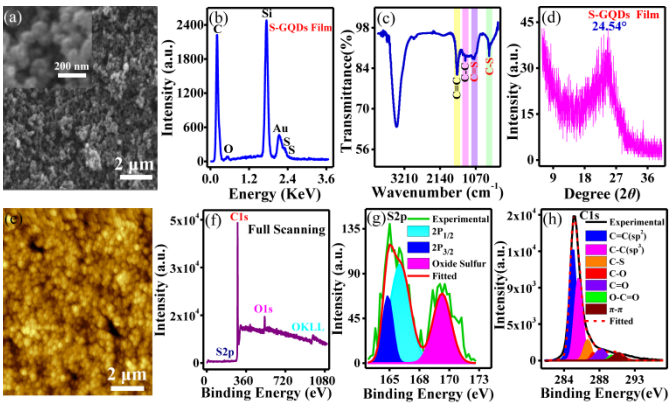

Fig. 2(a) SEM morphology of S-doped nanoparticles. Inset: An enlarged image to show the size and shape of nanoparticles. (b) EDS spectrum of the S-GQDs film on Si substrate. The Au peak came from the gold film sprayed on top of the surface. (c) FTIR spectrum of S-GQDs. (d) The XRD pattern of the S-GQDs. (e) AFM image of the S-GQDs film on Si substrate. (f) The full-scan XPS spectrum of the S-GQDs. (g) The XPS S2p spectrum of the S-GQDs. (h) The XPS C1s spectrum of the S-GQDs.

Pattern of the S-GQDs is shown in Fig. 2d. The peak at 2ϑ=24.5˚ corresponds to a *d*-spacing of 0.263 nm, which is substantially larger than that reported for un-doped GQDs.[21] This may be related to the sulphur doping with the sulphur-containing functional groups enlarging the basal planes separation.[22] The chemical composition of the S-GQDs is further analyzed using x-ray photoelectron spectroscopy (XPS). The full-scan XPS spectrum is shown in Fig. 2f. A dominant graphitic C1s peak at 282.8 eV, the O1s peak at 531 eV and S2p peak at 161.6 eV can be identified. As shown in Fig. 2g, the S2p spectrum can be deconvoluted into three peaks. The peak located at 169.1 eV is attributed to sulphur oxides-related bonds.[23,24] The peaks at 164.2 eV and 165.6 eV are related to the $S2p_{3/2}$ and $S2p_{1/2}$ orbitals respectively.[23,24] As shown in Fig. 2h, the C1s peak can be deconvoluted into seven peaks at 284.5 eV (C=C), 285.7 eV (C-C), 286.8 eV (C-O), 288.0 eV (C=O), 289.2 eV (O-C=O), and 290.8 eV (π-π interactions), in addition to the C-S peak at ~286.5 eV. The C-S peak is at a smaller binding energy than the C-O peak since oxygen is more electronegative than sulphur which makes the C-S bonds having a higher ionic character.[25] The C-S peak confirms again that sulphur is covalently doped into the graphitic structure.

Optical measurements are then carried out to investigate the modification on the optical properties of the GQDs after sulphur doping. The ultraviolet-visible (UV-Vis) absorption spectrum of S-GQDs aqueous solution is shown in Fig. 3c. There are two absorption peaks at 198 and 285 nm, comparing with un-doped GQDs with the two absorption peaks at ~230 and ~300 nm,[26-28] the absorption peaks of S-GQDs exhibit a blue shift of ~25nm, which indicates an increase in UV absorption after sulphur doping. The peak at 198 nm and the peak at 285 nm arises are probably due to S doped surface state region effectively modulated the bandgap of GQDs.

The photoluminescence excitation (PLE) spectrum of the S-GQDs as shown in Fig. 3c was measured by monitoring the

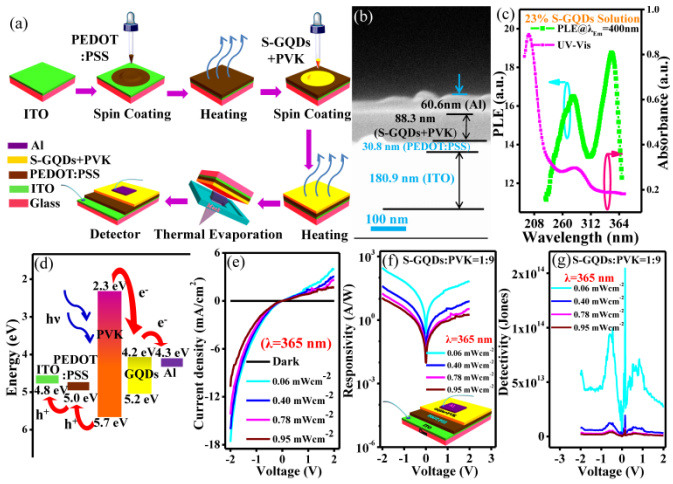

Fig. 3 (a) The schematic illustration for fabrication of PVK/S-GQDs hybrid UV detector. (b) The SEM cross-sectional image for the detector. (c) The UV-Vis and PLE spectra of S-GQD aqueous solution. (d) The schematic diagram of energy levels for the photovoltaic detector. (e) The *J–V* curves of the detector in the dark and under illumination at 365 nm with different light intensity. (f) The effect of UV illumination intensity (λ=365 nm) on responsivity. Inset: The schematic diagram of the PVK/S-GQDs hybrid UV detector. (g) The effect of UV illumination intensity (λ=365 nm) on detectivity.

emission at 400 nm. The PLE spectrum shows two peaks centered at 280 and 350 nm, which are different from the reported PLE peaks at 257-270 nm and 320-331 nm for the un-doped GQDs prepared from the hydrothermal reduction of graphene oxide[29] and chemical exfoliation method.[9] The difference in photon excitation energy in S-GQDs indicates that the sulphur-doping has induced changes in the electron energy level in the S-GQDs. Fig. S1 in the Supporting Information shows the photoluminescence (PL) spectra of the S-GQDs solution. The solution was excited by a Xe lamp in a fluorescence spectrometer. A broad emission peak at 427 nm was observed when the sample was excited at 300 nm. The PL peak shifted from 417 to 440 nm when the excitation wavelength was changed from 300 to 380 nm. The PL intensity decreased as the PL peak red-shifted. The dependence of the emission wavelength on the excitation wavelength is a commonly observed phenomenon in carbon-based QDs.[30-32]

To explore the potential of S-GQDs in optoelectronics, the S-GQDs based vertical junction photodetectors have been fabricated. Indium tin oxide (ITO)-coated glass was used as the substrate. The active layers of the devices composed of poly (9-vinylcarbazole) (PVK) mixed with S-GQDs (weight ratio of PVK to S-GQD is 9 to 1). Devices with PVK-sole active layer were also fabricated for comparison. The fabrication process of the device is schematically shown in Fig. 3a. The cross section of a typical device measured with SEM is shown in Fig. 3b. The thicknesses of the ITO anode, PEDOT:PSS, PVK:S-GQDs and Al cathode are 180.9, 30.8, 88.3, and 60.6 nm respectively. The PEDOT:PSS layer was adopted to facilitate hole transport in the device as PEDOT:PSS has a high work function, which can improve the hole injection towards the ITO anode.

The energy levels of different layers in the device are illustrated in Fig. 3d. For PVK, the LUMO and the HOMO are -2.3 and -5.7 eV respectively, with a bandgap (E_g) of 3.4 eV, [33-35] corresponding to the energy of the UV light. The HOMO and LUMO of the S-GQDs are calculated to be -5.2 and -4.2 eV respectively, with an E_g of 1.0 eV.[20,22] PVK is the major UV light absorber in the devices. Electron-hole pairs created in the PVK dissociate under the effect of applied bias, together with the assistance of a build-in electric field resulted from the energy difference of *HOMO*/*LUMO* between the layers, holes transport to the PEDOT:PSS layer then to the ITO anode while electrons transport to the S-GQDs and subsequently to Al cathode. S-GQDs facilitate electron transfer in the active layer.

Fig. 3e shows the current density-voltage (*J*-*V*) curves of the photodetector under UV illumination (λ=365 nm) with a series of light intensities (0.06, 0.40, 0.78 and 0.95 mWcm^{-2}). The device shows a remarkable increase in current density under illumination, which demonstrates that the detector exhibited an excellent photoresponse. Fig. 3f shows the bias voltage-dependent responsivity curves. The responsivity (R) is given by[36], $R = J_{ph}/P_{opt}$, where J_{ph} is photocurrent density which equals to the current density under illumination subtracting that in the dark; and P_{opt} is the incident light intensity. Under a forward bias voltage, R increases with the decrease in the intensity of the UV light. The responsivity was as high as 307 AW^{-1} under a light intensity of 0.06 mWcm^{-2}, which is 1.5x10^5 % higher than that of the PVK-sole control devices with a maximum R of 0.2 AW^{-1} (Fig. S2b, Supporting Information).

Detectivity (D^*) is another important parameter to evaluate the performance of a photodetector. D^* can be calculated as equation (1), [37]

$$D^* = R/\sqrt{2qJ_d} \quad (1)$$

Where J_d is the dark current density and q the electron charge. The voltage dependent D^* curves are shown in Fig. 3g. D^* increases with decreasing light intensity. The highest D* reached 1.5x10^{14} Jones under a light intensity of 0.06 mWcm^{-2}, which also has a higher performance by 5.8x10^4 % when compared to the PVK-sole control device with a maximum D^* of 2.6x10^{11}Jones (Fig.S2c), in the supplementary material). It is found that the illumination intensity may affect D^*. For our device, D^* increases with a decrease in the illumination intensity, implying that our device is suitable for detecting weak light intensity. The greatly enhanced R and D^* after the incorporation of S-GQDs clearly demonstrated the important role of S-GQDs for facilitating electron transport and thereby preventing recombination of carriers in the device.

In the above experiments, the S-GQDs were prepared by a newly invented co-combustion method (T-X-J Method) using a mixture of paraffin liquid and CS_2 as the precursors. Paraffin liquid plays two important roles during the preparation of S-GQDs. One is to act as a carbon source, and the other is to provide energy to sustain the combustion. CS_2 is to provide a S-doping source.5 g of liquid paraffin and 1 g of CS_2 were uniformly mixed under stirring in a beaker, the solution was then poured into an alcohol burner, and was ignited with a cotton wick. A glass slide was placed above the flame, black soot was collected on the glass slide. 0.25 g of soot was

scratched from the slide, then 50 mL of NMP was added. The mixture was sonicated for 5 hours with a frequency of 53 kHz, followed by centrifugation at 8000 rpm for 25 min. The supernatant was collected to give the S-GQDs solution, and the S-GQDs powders were obtained after evaporating the solvent at 80°C.

The detector fabrication process is a 100 ml chlorobenzene solution containing 0.5 g of S-GQDs powders and 4.5 g PVK was made. The solution was sonicated for 6 h and then magnetic stirred for 2 days. Indium tin oxide (ITO) coated glass substrates (Hefei Kejing), used as transparent bottom electrode, was first cleaned by chemical bath method using a solution containing H_2O:H_2O_2:$NH_3{\cdot}H_2O$ (2 : 1 : 1) in a hot water bath at 80°C for 30 min and then dried under air flow. PEDOT:PSS solution was first spin-coated onto the ITO substrates at 2000 rpm. After being dried at 80°C for 15 min, PVK/S-GQDs solution in chlorobenzene was spin-coated on top of the PEDOT:PSS layer at 2000 rpm for 30 s, to give the active layers of the photovoltaic devices. Al electrodes, acted as top electrodes, were deposited by thermal evaporation under vacuum (~2.3×10^{-4}Pa). Control devices with the PVK-only active layer were prepared using a similar process but with the replacement of S-GQDs by PVK of the same mass.

Conclusions

In conclusion, the use of the co-combustion of CS_2 and liquid paraffin mixture in a low-cost alcohol lamp for the all-green synthesis of S-GQDs is realized for the first time. The S-GQDs has a small size distribution with an average diameter of 2.46 nm. The good crystallinity and low defect density have been confirmed with TEM and Raman spectrum. The sulphur doping has effectively adjusted the optical absorption of S-GQDs to enhance the absorption in UV region, such that high performance UV photodetectors based on the S-GQDs:PVK have been fabricated. The responsivity of the devices was as high as 307 AW^{-1}, with an excellent detectivity of 1.5×10^{14} Jones at 365 nm illumination, which significantly outperform the control devices without S-GQDs. This study shines light on the green and facile synthesis of GQDs which can at the same time allow effective doping in the GQDs. GQDs with other doping elements are anticipated to be produced in a similar way by choosing appropriate precursors. In this way the optical properties of the GQDs can be tuned to vary the detection wavelength of the GQDs-based solution processable photodetectors for different applications.

Acknowledgements

This work was supported by National Natural Science Foundation of China (Nos. 61106098 and 51201150), the Key Project of Applied Basic Research of Yunnan Province, China (No. 2012FA003).

Notes and references

1 N. Prabhakar, T. Nareoja, E. von Haartman, D. SenKaraman, S. A. Burikov, T. A. Dolenko, T. Deguchi, V. Mamaeva, P. E. Hanninen, I. I. Vlasov, O. A. Shenderova and J. M. Rosenholm ， Nanoscale, 2015, **7**, 10410-10420.
2 L. B. Tang, R. B. Ji, X. K. Cao, J. Y. Lin, H. X. Jiang, X. M. Li, K. S. Teng, C. M. Luk, S. J. Zeng, J. H. Hao and S. P. Lau, ACS Nano, 2012, **6**, 5102–5110.
3 Y. Li, Y. Hu, Y. Zhao, G. Q. Shi, L. Deng, Y. B. Hou and L. T. Qu, Adv. Mater., 2011, **23**, 776–780.
4 J. Jasieniak, M. Califano and S. E. Watkins, ACS Nano, 2011, **7**, 5888–5902.
5 P. V. Kamat, Acc. Chem. Res., 2012, **45**, 1906–1915.
6 A. J. Nozik, M. C. Beard, J. M. Luther, M. Law, R. J. Ellingson and J. C. Johnson, Chem. Rev., 2010, **110**, 6873–6890.
7 G. M. Wang, X. Y. Yang, F. Qian, J. Z. Zhang and Y. Li, Nano Lett., 2010, **10**, 1088–1092.
8 X. M. Li, S. P. Lau, L. B. Tang, R. B. Ji and P. Z. Yang, Nanoscale, 2014, **6**, 5323–5328.
9 S. K. Lai, C. M. Luk, L. B. Tang, K. S. Teng and S. P. Lau, Nanoscale, 2015, **7**, 5338-5343.
10 P. Huang, J.-J. Shi, M. Zhang, X.-H. Jiang, H.-X. Zhong, Y.-M. Ding, X. Cao, M. Wu and J. Lu, J. Phys. Chem. Lett., 2016, **7**, 2888-2892.
11 B. H. Park, S. J. Kim, J. S. Sohn, M. S. Nam, S. Kang and S. C. Jun, Nano Res., 2016, **9**, 1866–1875.
12 X. S. Li, W. W. Cai, J. H. An, S. Kim, J. Nah, D. X. Yang, R. Piner, A. Velamakanni, I. Jung, E. Tutuc, S. K. Banerjee, L. Colombo and R. S. Ruoff, Science, 2009, **324**, 1312–1314.
13 P. Y. Huang, C. S. Ruiz-Vargas, A. M. van der Zande, W. S. Whitney, M. P. Levendorf, J. W. Kevek, S. Garg, J. S. Alden, C. J. Hustedt, Y. Zhu, J. Park, P. L. McEuen and D. A. Muller, Nature, 2011, **469**, 389–392
14 F. Bonaccorso, Z. Sun, T. Hasan and A. C. Ferrari, Nat. Photonics, 2010, **4**, 611–622.
15 J. C. Meyer, S. Kurasch, H. J. Park, V. Skakalova, D. Künzel, A. Groß, A. Chuvilin, G. Algara-Siller, S. Roth, T. Iwasaki, U. Starke, J. H. Smet and U. Kaiser, Nat. Mater., 2011, **10**, 209-215.
16 J. H. Zhao, L. B. Tang, J. Z. Xiang, R. B. Ji, Y. B. Hu, J. Yuan, J. Zhao, Y. J. Tai and Y. H. Cai, RSC Adv., 2015, **5**, 29222–29229.
17 L. B. Tang, R. B. Ji, X. M. Li, K. S. Teng and S. P. Lau, Part. Part. Syst. Charact., 2013, **30**, 523-531.
18 X.-W. Fu, Z.-M. Liao, Y.-B. Zhou, H.-C. Wu, Y.-Q. Bie, J. Xu and D.-P. Yu, Appl. Phys. Lett., 2012, **100**, 223114.
19 L. B. Tang, X. M. Li, R. B. Ji, K. S. Teng, G. Tai, J. Ye, C. S. Wei and S. P. Lau, J. Mater. Chem., 2012, **22**, 5676–5683.
20 S. K. Lai, L. B. Tang, Y. Y. Hui, C. M. Luk and S. P. Lau, J. Mater. Chem. C, 2014, **2**, 6971-6977.
21 Y. Q. Dong, C. Q. Chen, X. T. Zheng, L. L. Gao, Z. M. Cui, H. B. Yang, C. X. Guo, Y. W. Chi and C. M. Li, J. Mater. Chem., 2012, **22**, 8764–8766.
22 J. H. Zhao, L. B. Tang, J. Z. Xiang, R. B. Ji, J. Yuan, J. Zhao, R. Y. Yu, Y. J. Tai and L. Y. Song, Appl. Phys. Lett., 2014, **105**, 111116.
23 S. B. Yang, L. J. Zhi, K. Tang, X. L. Feng, J. Maier and K. Müllen, Adv. Funct. Mater., 2012, **22**, 3634–3640.
24 D. Qu, M. Zheng, P. Du, Y. Zhou, L. G. Zhang, D. Li, H. Q. Tan, Z. Zhao, Z. G. Xie and Z. C. Sun, Nanoscale, 2013, **5**, 12272–12277.
25 H. L. Poh, P. Šimek, Z. Sofer and M. Pumera, ACS Nano, 2013, **7**, 5262–5272.
26 S. J. Zhu, Y. B. Song, J. R. Shao, X. H. Zhao and B. Yang, Angew. Chem., Int. Ed., 2015, **54**, 14626 – 14637.
27 M. Zhang, L. L. Bai, W. H. Shang, W. J. Xie, H. Ma, Y. Y. Fu, D. C. Fang, H. Sun, L. Z. Fan， M. Han, C. C. Liu and S. H. Yang, J. Mater. Chem., 2012, **22**, 7461–7467.
28 L. X. Lin and S. W. Zhang, Chem. Commun., 2012, **48**, 10177–10179.

29 D. Pan, J. C. Zhang, Z. Li and M. H. Wu, Adv. Mater., 2010, **22**, 734–738.
30 J. H. Shen, Y. H. Zhu, C. Chen, X. L. Yang and C. Z. Li, Chem. Commun., 2011, **47**, 2580–2582.
31 R. l. Liu, D. Q. Wu, X. L. Feng and K. Müllen, J. Am. Chem. Soc., 2011, **133**, 15221–15223.
32 J. H. Shen, Y. H. Zhu, X. L. Yang, J. Zong, J. M. Zhang and C. Z. Li, New J. Chem., 2012, **36**, 97–101.
33 F. X. Meng, L. Shen, Y. F. Wang, S. P. Wen, X. H. Gu, J. R. Zhou, S. Tian and S. P. Ruan, RSC Adv., 2013, **3**, 21413–21417.
34 D.-C. Perng, H.-P. Lin and M.-H. Hong, Appl. Phys. Lett., 2015, **107**, 241113.
35 S.-W. Lee, S.-H. Cha, K.-J. Choi, B.-H. Kang, J.-S. Lee, S.-W. Kim, J.-S. Kim, H.-M. Jeong, S.-A. Gopalan, D.-H. Kwon and S.-W. Kang, Sensors, 2016, **16**, s16010074.
36 S. K. Lai, C. Xie, K. S. Teng, Y. Li, F. Tan, F. Yan and S. P. Lau, Adv. Optical Mater., 2016, **4**, 555-561.
37 X. Gong, M. H. Tong, Y. J. Xia, W. Z. Cai, J. S. Moon, Y. Cao, G. Yu, C.-L. Shieh, B. Nilsson and A. J. Heeger, Science, 2009, **325**, 1665-1667.